arXiv:2506.19329v1 [cs.LG] 24 Jun 2025

Contrastive Cross-Modal Learning for Infusing Chest X-ray Knowledge into ECGs

Vineet Punyamoorty VPUNYAMO@PURDUE.EDU
Elmore Family School of Electrical and Computer Engineering
Purdue University
West Lafayette, IN 47907, USA

Aditya Malusare MALUSARE@PURDUE.EDU
Edwardson School of Industrial Engineering
Purdue University
West Lafayette, IN 47907, USA

Vaneet Aggarwal VANEET@PURDUE.EDU
Edwardson School of Industrial Engineering
Purdue University
West Lafayette, IN 47907, USA

Abstract

Modern diagnostic workflows are increasingly multimodal, integrating diverse data sources such as medical images, structured records, and physiological time series. Among these, electrocardiograms (ECGs) and chest X-rays (CXRs) are two of the most widely used modalities for cardiac assessment. While CXRs provide rich diagnostic information, ECGs are more accessible and can support scalable early warning systems. In this work, we propose CroMoTEX, a novel contrastive learning-based framework that leverages chest X-rays during training to learn clinically informative ECG representations for multiple cardiac-related pathologies: cardiomegaly, pleural effusion, and edema. Our method aligns ECG and CXR representations using a novel supervised cross-modal contrastive objective with adaptive hard negative weighting, enabling robust and task-relevant feature learning. At test time, CroMoTEX relies solely on ECG input, allowing scalable deployment in real-world settings where CXRs may be unavailable. Evaluated on the large-scale MIMIC-IV-ECG and MIMIC-CXR datasets, CroMoTEX outperforms baselines across all three pathologies, achieving up to 78.31 AUROC on edema. Our code is available at github.com/vineetpmoorty/cromotex.

Keywords: multimodal learning, contrastive learning, cross-modal learning

1 Introduction

Cardiovascular diseases are the leading cause of mortality worldwide, emphasizing the need for reliable and scalable diagnostic tools. The growing availability of multimodal medical data presents an opportunity for cross-modal knowledge transfer, which can enable earlier and more accessible diagnosis by leveraging inexpensive, widely available modalities in place of less accessible gold-standard tests. Among commonly used diagnostic modalities, chest X-rays (CXRs) provide detailed anatomical insights but require hospital-based imaging and specialized equipment, making them less accessible. Electrocardiograms (ECGs), in contrast, are widely available, especially with the rise of wearable technology, and facilitate

©2025 Vineet Punyamoorty, Aditya Malusare and Vaneet Aggarwal.
License: CC-BY 4.0, see https://creativecommons.org/licenses/by/4.0/.

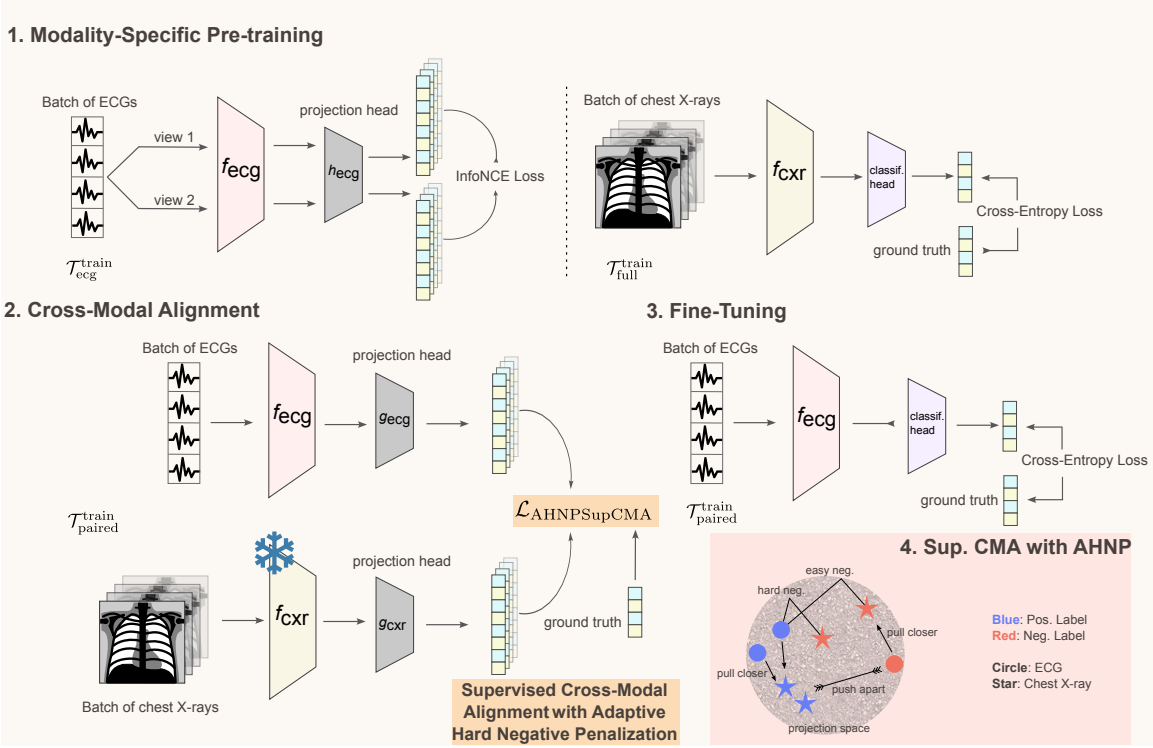


Figure 1: CROMOTEX consists of modality-specific encoders f_{ecg} and f_{cxr}, along with respective projection and classification heads. **1.** We first pre-train f_{ecg} in a self-supervised fashion, and pre-train f_{cxr} on the disease label. **2.** We next perform supervised cross-modal alignment by infusing the knowledge from f_{cxr} to learn rich, task-relevant ECG representation and then **3.** fine-tune the ECG encoder on the disease labels. **4.** We propose $\mathcal{L}_{\text{AHNPSupCMA}}$, a novel loss function that uses Adaptive Hard Negative Penalization (AHNP) to allocate higher weights to the losses arising from hard negatives (Sec. 3.2).

early screening. However, ECGs alone often lack the anatomical detail necessary for robust diagnosis, limiting their effectiveness. Given the complementary nature of CXRs and ECGs, transferring knowledge from CXRs to ECGs could enhance ECG-based disease detection, improving early diagnosis and patient outcomes. Despite this potential, little research has explored this direction, with most prior research on multimodal ECG learning focusing on multimodal fusion with other modalities (Hayat et al., 2023; Yao et al., 2024; Thapa et al., 2024) and alignment with clinical text for zero-shot classification (Liu et al., 2024). ECCL (Ding et al., 2024) and Cross-modal Autoencoder (Radhakrishnan et al., 2023) explore cross-modal transfer from Cardiac Magnetic Resonance Imaging (CMR) to ECG. However, they rely on CMR, a significantly more resource-intensive imaging modality compared to CXR, limiting its scalability and accessibility. Furthermore, they employ a simple alignment strategy that only aligns ECG-CMR pairs from the same sample, disregarding other semantically similar pairs that share the same disease label. Introducing supervision in the alignment process could help the model fully leveraging large labeled datasets, promoting it to learn more generalizable and task-relevant ECG representations.

In this paper, we propose CROMOTEX (**Cro**ss-**Mo**dal **T**ransfer between **E**CG and Chest **X**-ray), a novel supervised cross-modal learning framework that facilitates knowledge transfer from CXRs to ECGs. To address the limitations of prior work, we propose a supervised contrastive alignment strategy that explicitly incorporates disease labels to guide ECG representation learning. To further improve the quality of alignment, we introduce a novel contrastive loss function with adaptive hard negative penalization (AHNP), which dynamically re-weights negative ECG-CXR pairs based on similarity, effectively penalizing harder negatives more and improving the alignment process.

We evaluate our approach on three clinically significant conditions: Cardiomegaly, Pleural Effusion, and Edema. Cardiomegaly, or heart enlargement, is typically diagnosed via chest X-ray but may manifest subtle cardiac signals detectable in ECG. Pleural Effusion, the accumulation of fluid in the pleural cavity, and Edema, fluid retention often associated with heart failure, are both visually prominent on CXRs but may induce indirect electrical patterns measurable by ECG. Studying these pathologies allows us to investigate the viability of ECG-based prediction for conditions where CXRs provide diagnostic gold standards—making them ideal candidates for evaluating cross-modal knowledge transfer.

The key contributions of our work are:

1. A novel supervised cross-modal learning framework for transferring knowledge from CXRs to ECGs, leveraging disease labels for task-relevant and generalizable representation learning

2. A new contrastive loss function, $\mathcal{L}_{\text{AHNPSupCMA}}$, which adaptively penalizes harder negatives, improving ECG-CXR alignment

3. Ablation studies validating the effectiveness of self-supervised ECG pre-training, supervised cross-modal alignment, and similarity-based hard negative penalization in our pipeline.

2 Related Work

2.1 Contrastive Learning

Contrastive learning involves self-supervised learning of representation by maximizing the alignment between projected embeddings of augmented views of the same sample, while simultaneously minimizing the alignment between those of different samples, using the InfoNCE loss (Oord et al., 2018). This enables the encoder to learn meaningful representations from datasets with little to no labeled data while promoting feature learning that generalizes effectively across diverse downstream tasks. Notable approaches include SimCLR (Chen et al., 2020), which maximizes the agreement between augmented views using a simple framework with a large batch size and a projection head; MoCo (He et al., 2020), which introduces a momentum-based memory bank to maintain a dynamic queue of negative samples for contrastive learning; and BYOL (Grill et al., 2020), which departs from explicit negative samples by relying on a momentum encoder and a predictor network to learn robust representations in a self-distilled manner.

2.2 Multimodal Contrastive Learning with Images

Multimodal representation learning aligns samples from one modality with semantically related samples from another, enabling both to be represented in a shared embedding space. This facilitates downstream tasks such as cross-modal retrieval and zero-shot classification. A prominent example is CLIP (Radford et al., 2021), which learns joint image-text representations by aligning images with their corresponding textual descriptions to enable flexible retrieval and zero-shot transfer. ALIGN (Jia et al., 2021) extends this idea to massive image-text pairs, further improving generalization across diverse datasets.

2.3 Multimodal Learning in Healthcare

Multimodal learning has emerged as a powerful paradigm in healthcare, enabling models to integrate heterogeneous data sources such as imaging, waveforms, structured clinical data, and free-text notes. The central goal is to improve clinical decision-making by leveraging the complementary strengths of different modalities.

GLoRIA (Huang et al., 2021) is a foundational effort in this space, aligning chest X-ray images with their corresponding radiology reports through a contrastive learning framework. By jointly training vision and language encoders, the model learns clinically meaningful representations that enable zero-shot classification and improved report retrieval. This highlights how multimodal learning can bridge the gap between visual evidence and textual reasoning. Hager et al. (Hager et al., 2023) extend this idea by fusing imaging data with structured clinical variables (e.g., age, sex, lab tests), demonstrating that integrating tabular features can enhance performance in disease classification tasks compared to image-only models. King et al. (King et al., 2023) take a different approach by aligning continuous clinical measurements (e.g., vital signs, labs) with unstructured clinical notes using a contrastive loss. This strategy improves the quality of learned representations for ICU outcome prediction, even in the absence of labels, reinforcing the power of contrastive learning to extract useful supervision from weakly paired data.

Other recent studies such as Thapa et al. (Thapa et al., 2024) and Ding et al. (Ding et al., 2024) explore modality alignment at a fine-grained level. These works demonstrate the effectiveness of contrastive learning in aligning representations across diverse inputs such as EHR, ECG, and imaging. Together, these efforts suggest that multimodal learning—particularly when paired with contrastive objectives—holds significant promise for developing holistic, generalizable patient models.

2.4 Contrastive Learning on ECGs and Chest X-rays

Contrastive learning has proven to be a highly effective method for self-supervised representation learning, especially in medical domains where labeled data is scarce but raw signals and images are abundant. Within this context, ECGs and chest X-rays are two high-value modalities due to their ubiquity and diagnostic relevance.

For ECGs, models like CLOCS (Kiyasseh et al., 2021) leverage contrastive learning on augmented views of raw ECG waveforms. By training on tasks such as segment-level and lead-wise discrimination, CLOCS learns representations that generalize well to downstream tasks including cardiovascular disease classification and arrhythmia detection. Similarly, Cheng et al. (Cheng et al., 2020) propose a subject-aware contrastive framework that improves ECG representations by contrasting signals from the same subject across time, which leads to better patient-level phenotyping.

On the imaging side, Sowrirajan et al. (Sowrirajan et al., 2021) propose MoCo-CXR, an adaptation of Momentum Contrast (MoCo) (He et al., 2020) for chest X-ray representation learning. Their model uses large-scale unlabeled CXR data to pre-train an encoder that significantly boosts performance on downstream classification tasks, such as identifying pulmonary conditions from frontal X-rays.

Additionally, CIA-Net (Liu et al., 2019) introduces contrastive induced attention mechanisms to improve localization of abnormalities in CXRs. This model explicitly encourages attention maps to align across augmented views, improving both classification and interpretability.

These advances collectively illustrate how contrastive learning—whether applied to time-series data like ECGs or spatial modalities like chest X-rays—can uncover robust and transferable representations. In particular, the potential to align these two modalities under a unified contrastive framework opens new opportunities for cross-modal learning and generalization across diagnostic tools.

3 Methods

3.1 Problem Setup: Supervised Cross-Modal Contrastive Learning

We propose a combination of CLIP-style (Radford et al., 2021) cross-modal alignment and SupCon-style (Khosla et al., 2020) supervised objective to perform supervised cross-modal contrastive learning as described below. Given a labeled dataset $\mathcal{D}_{\text{paired}}$ of ECGs (e_i), chest X-rays (x_i) and disease labels (y_i), $\mathcal{D}_{\text{paired}} = \{e_i, x_i, y_i\}_{i=1}^{N}$, our goal is to learn representations for the two modalities by contrasting positive pairs against negative pairs. As seen in Fig. 1, we have modality-specific encoders f_{ecg}, f_{cxr} and projection heads g_{ecg}, g_{cxr} which project the embeddings onto a common space. Given a batch $\mathcal{B}$ of samples $\{e_i, x_i, y_i\}_{i=1}^{B}$,

after obtaining the projected embeddings $z_i^e = g_{\text{ecg}}(f_{\text{ecg}}(e_i))$ and $z_i^x = g_{\text{cxr}}(f_{\text{cxr}}(x_i))$ one can train the network consisting of $f_{\text{cxr}}, f_{\text{ecg}}, g_{\text{cxr}}$ and g_{ecg} using the following cross-modal alignment objective:

$$\mathcal{L}_{\text{CMA}} = \frac{-1}{2}\sum_{i=1}^{B}\log\frac{\exp(z_i^e \cdot z_i^x/\tau)}{\sum_{a\in A(i)}\exp(z_i^e \cdot z_a^x/\tau)} - \frac{1}{2}\sum_{i=1}^{B}\log\frac{\exp(z_i^x \cdot z_i^e/\tau)}{\sum_{a\in A(i)}\exp(z_i^x \cdot z_a^e/\tau)} \tag{1}$$

where $A(i) = \mathcal{B} \setminus \{i\}$. This objective is a symmetrized version (Ding et al., 2024) of InfoNCE loss (Oord et al., 2018) and it aims to align the projected embeddings of the two modalities from the same sample (e_i, x_i) while simultaneously pushing apart the projections from different samples (e_i, x_j) for all $i \neq j$. However, this objective does not use supervision from the available labels y_i and therefore does not account for the task-relevant, semantically positive pairs from different samples: $\{(e_i, x_j) : y_i = y_j, i \neq j\}$. To address this, following SupCon (Khosla et al., 2020), we have the objective $\mathcal{L}_{\text{SupCMA}} = \frac{1}{2}\mathcal{L}_{\text{SupCMA}}^{e,x} + \frac{1}{2}\mathcal{L}_{\text{SupCMA}}^{x,e}$ where

$$\mathcal{L}_{\text{SupCMA}}^{m,n} = -\sum_{i=1}^{B}\frac{1}{|P(i)|}\sum_{p\in P(i)}\log\frac{\exp(z_i^m \cdot z_p^n/\tau)}{\sum_{a\in A(i)}\exp(z_i^m \cdot z_a^n/\tau)} \tag{2}$$

$P(i) = \{p \in A(i) : y_p = y_i\}$ represents the set of all positive pairs obtained by matching the label y.

3.2 Supervised Contrastive Loss with Adaptive Hard Negative Penalization

In the supervised objective described above (Eqn. 2), a sample pair (e_i, x_j) with different labels $(y_i \neq y_j)$ can be termed as a *negative*. However, not all negatives are equal—*hard negatives*, i.e. pairs $\{(e_i, x_j) : e_i, x_j \in \mathcal{B}\}$ with high similarity $z_i^e \cdot z_j^x$ in the projection space while having different labels $y_i \neq y_j$, are particularly challenging. Therefore, it could help to prioritize the losses arising from hard negatives more strongly than those from easy ones. To address this problem, we propose to modify $\mathcal{L}_{\text{SupCMA}}$ by performing weighted summation of the negative-pair terms in the denominator of Eqn. 2, such that hard negatives are assigned higher weights, which we call **a**daptive **h**ard **n**egative **p**enalization (AHNP):

$$\mathcal{L}_{\text{AHNPSupCMA}}^{m,n} = -\sum_{i=1}^{B}\frac{1}{|P(i)|}\sum_{p\in P(i)}\log\frac{(1+\beta\mathbb{1}_{i=p})\exp(z_i^m \cdot z_p^n/\tau)}{\sum_{a\in A(i)} w_{i,a}\exp(z_i^m \cdot z_a^n/\tau)} \tag{3}$$

where $w_{i,a} = \text{w}(z_i^m \cdot z_a^n/\tau)$ is the weighting function.

To implement adaptive hard negative penalization, we define a weighting function $w_{i,a}$ that determines how strongly each negative sample $a \in A(i)$ contributes to the denominator of the contrastive loss for a given anchor z_i^m. We explore three different weighting strategies—`linear`, `topk`, and `exp`—each designed to emphasize harder negatives (i.e., those with higher similarity to the anchor) more than easier ones.

- `linear` strategy: The weights are scaled linearly based on similarity. For each anchor z_i^m, we compute the similarity with every other sample in the batch and linearly assign weights $w_{i,a}$ such that samples with higher similarity receive larger weights. Specifically, the weights are distributed from 1 up to a maximum value $\alpha > 1$, with α controlling the strength of this emphasis.

- `topk` strategy: For each anchor z_i^m, we identify the top $k\%$ of samples (in terms of similarity) and assign them a fixed higher weight $\alpha > 1$, while all other samples receive a default weight of 1. This sharply focuses the contrastive loss on the hardest negatives in the batch, leaving easier negatives largely unaffected.

- `exp` strategy: We employ an exponential function to assign weights. Each weight is computed as $w_{i,a} = 1+\exp(\alpha \cdot z_i^m \cdot z_a^n)$, where α controls the steepness of the exponential curve. This strategy creates a highly nonlinear weighting profile in which even small increases in similarity between anchor and negative can result in a significant increase in penalty.

In all three strategies, α (and k for `topk`) are treated as tunable hyperparameters that govern how aggressively the model prioritizes hard negatives during training.

In addition to AHNP, we also assign higher weight β ($\beta > 1$) to within-sample cross-modal positive pairs in the numerator of our contrastive loss, to encourage stronger alignment between inherently corresponding ECG and CXR representations. This extra weighting for within-sample cross-modal pairs allows us to tune the loss function between two extremes: one where no supervision from labels is used (at high values of β, the extra weight given to within-sample pairs) and another where all same-label pairs are treated equally.

We use the objective $\mathcal{L}_{\text{AHNPSupCMA}} = \frac{1}{2}\mathcal{L}^{e,x}_{\text{AHNPSupCMA}} + \frac{1}{2}\mathcal{L}^{x,e}_{\text{AHNPSupCMA}}$ in this work.

Algorithm 1 Supervised Cross-Modal Contrastive Learning with Adaptive Hard Negative Penalization

Require: Paired dataset $\mathcal{D}_{\text{paired}} = \{(e_i, x_i, y_i)\}_{i=1}^{N}$, ECG-only dataset $\mathcal{T}_{\text{ecg}}^{\text{train}}$, pre-trained weights for f_{cxr}

Require: Hyperparameters: temperature τ, weights α, β, batch size B, top-k, learning rates

procedure PRETRAIN($f_{\text{cxr}}, f_{\text{ecg}}$)
  Train f_{cxr} on cardiomegaly labels using cross-entropy loss
  Train f_{ecg} with SimCLR-style contrastive learning on $\mathcal{T}_{\text{ecg}}^{\text{train}}$
  Discard projection head h_{ecg} after training
  Freeze f_{cxr}
end procedure
procedure CROSSMODALALIGNMENT
  for each training step **do**
    Sample batch $\mathcal{B} = \{(e_i, x_i, y_i)\}_{i=1}^{B}$ using weighted random sampler
    Compute $z_i^e = g_{\text{ecg}}(f_{\text{ecg}}(e_i))$, $z_i^x = g_{\text{cxr}}(f_{\text{cxr}}(x_i))$ for all i
    for each anchor $i = 1$ to B **do**
      $P(i) \leftarrow \{p \neq i \mid y_p = y_i\}$
      $A(i) \leftarrow \mathcal{B} \setminus \{i\}$
      for each $a \in A(i)$ **do**
        Compute similarity $s_{i,a} \leftarrow z_i^m \cdot z_a^n$
        Compute weight $w_{i,a}$ using chosen AHNP strategy:
        if `linear` **then** $w_{i,a} \propto$ rank of $s_{i,a}$
        else if `topk` **then** $w_{i,a} \leftarrow \alpha$ if $a \in$ top-k similar; else 1
        else if `exp` **then** $w_{i,a} \leftarrow 1 + \exp(\alpha \cdot s_{i,a})$
        end if
      end for
      Compute loss $\mathcal{L}_i$ using weighted SupCon-style formulation with β emphasis on within-sample pairs
    end for
    Compute total loss: $\mathcal{L}_{\text{AHNPSupCMA}} \leftarrow \frac{1}{2}\sum_i \mathcal{L}_i^{e,x} + \frac{1}{2}\sum_i \mathcal{L}_i^{x,e}$
    Update f_{ecg}, g_{ecg}, g_{cxr} using `AdamW`, cosine LR decay, and gradient clipping
  end for
end procedure
procedure FINETUNE(f_{ecg})
  Discard projection heads $g_{\text{ecg}}, g_{\text{cxr}}$
  Fine-tune f_{ecg} on cardiomegaly labels using cross-entropy loss
  Use same class-balanced sampling as in alignment phase
end procedure

3.3 Model and Training Details

Our model consists of an ECG encoder f_{ecg}, chest X-ray encoder f_{cxr} and linear projection heads g_{ecg} and g_{cxr} (Fig. 1). We implement f_{ecg} as a series of two 1-D convolution layers, each consisting of ReLU activation and 1D `BatchNorm`, followed by a Transformer encoder

consisting of 8 attention heads, 4 Transformer blocks (Vaswani et al., 2017) and 1D Adaptive Pooling to obtain the ECG embeddings $f_{\text{ecg}}(e_i)$.

For the chest X-ray image encoder f_{cxr}, we use a DenseNet-121 model pre-trained on MIMIC-CXR data from TorchXRayVision (Cohen et al., 2022). We replace the original multi-label classification head with a single-label and further train it for disease label prediction.

3.3.1 Pre-training

We first pre-train the modality-specific encoders f_{ecg} and f_{cxr}. f_{cxr} is pre-trained using $\mathcal{T}_{\text{full}}^{\text{train}}$ and $\mathcal{T}_{\text{full}}^{\text{val}}$ with Cross-Entropy loss on the disease labels using initial weights from TorchXRayVision (Cohen et al., 2022). We use the `Adam` optimizer with peak learning rate (LR) of 10^{-4}, batch size 64, a learning rate scheduler with linear warm-up for 10 epochs from LR of 10^{-5}, and gradual cosine decay back to 10^{-5}. The backbone's LR is scaled by 0.05 times relative to the classification head to preserve features learned from TorchXRayVision's pre-training.

To pre-train the ECG encoder f_{ecg}, we perform self-supervised learning (SSL) using the datasets $\mathcal{T}_{\text{ecg}}^{\text{train}}$ and $\mathcal{T}_{\text{ecg}}^{\text{val}}$ following the SimCLR technique (Chen et al., 2020) to help it learn generalizable ECG features. We use a linear projection head h_{ecg} to align the projected embeddings of two augmented views of each ECG in a batch using InfoNCE loss, following which h_{ecg} is discarded. We use VCG-based augmentations for the pre-training, as described in Sec. 4.1.

3.3.2 Cross-modal Alignment

Once both the modality-specific encoders f_{ecg} and f_{cxr} are pre-trained, we freeze the chest X-ray encoder f_{cxr} for all further steps. This ensures that f_{cxr} serves as a teacher in the cross-modal alignment process, where we learn ECG representation in alignment with the frozen chest X-ray embeddings. We find in our experiments that un-freezing f_{cxr} leads to poor downstream performance. For cross-modal alignment, we use modality specific projection heads g_{cxr} and g_{ecg} as shown in Fig. 1 to align the projected embeddings of the two modalities using our supervised cross-modal alignment objective with adaptive hard negative penalization, $\mathcal{L}_{\text{AHNPSupCMA}}$ (Eqn. 3). We use the `AdamW` optimizer with peak LR of 10^{-4}, batch size of 256, linear warm-up for 10 epochs from LR 10^{-5}, followed by gradual cosine decay to 10^{-5}. We set weight decay to 10^{-5} and clip gradients to 2.5 for training stability. The learning rate for both projection heads is scaled by 0.1 times relative to that of f_{ecg}, as they are simple linear layers. To help mitigate the effect of high class imbalance in the dataset, we use `WeightedRandomSampler` with replacement to over-sample from the minority class ($y_i = 1$) to ensure they constitute $25 - 30\%$ of each batch. To help the model learn generalizable ECG representation, we use the time-domain ECG augmentations described in (Raghu et al., 2022).

3.3.3 Fine-tuning

Finally, we discard the projection heads g_{ecg}, g_{cxr} and fine-tune the ECG encoder f_{ecg} on the disease labels with a Cross-Entropy objective, and continue to over-sample from the minority class as describe above. We use the `Adam` optimizer with peak LR of 10^{-5}, batch

size of 256, linear warm-up for 10 epochs from LR 10^{-6}, followed by gradual cosine decay to 10^{-6}. We obtain the optimal hyperparameters from the best fine-tuning AUROC results as follows: $\tau = 0.01$, `topk` AHNP, with $k = 7.5\%$, $\alpha = 4.5$ and $\beta = 2$, refer Eqn. 3.

We summarize all model and training hyperparameters in Table 3, and the training procedure in Algorithm 1.

4 Experiment and Results

Table 1: Performance comparison of CROMOTEX against baselines, along with ablation studies for three pathologies. We also show the metrics for CXR-based classification using f_{cxr} at the bottom for reference.

Model	**Cardiomegaly**		**Edema**		**Pleural Effusion**	
	AUROC ↑	F1 ↑	AUROC ↑	F1 ↑	AUROC ↑	F1 ↑
Direct Classif. (ECG)	72.84 ± 0.51	30.31 ± 0.21	74.89 ± 0.36	18.11 ± 0.28	72.20 ± 0.38	20.18 ± 0.19
ResNet-1D	70.65 ± 0.22	28.24 ± 0.41	68.42 ± 0.30	17.42 ± 0.30	63.51 ± 0.41	17.99 ± 0.34
ECCL (Ding et al., 2024)	70.85 ± 0.14	27.47 ± 0.13	67.87 ± 0.91	13.68 ± 0.31	64.12 ± 0.67	17.81 ± 0.28
BIOT (Yang et al., 2023)	72.63 ± 0.02	30.17 ± 0.05	69.45 ± 0.33	13.84 ± 0.61	60.23 ± 0.10	16.52 ± 0.13
SupCon (Khosla et al., 2020)	74.46 ± 0.16	31.42 ± 0.31	77.64 ± 0.38	20.15 ± 0.12	70.81 ± 0.20	25.98 ± 0.59
Cross-modal AE (Radhakrishnan et al., 2023)	72.15 ± 0.13	28.31 ± 0.79	68.26 ± 0.42	13.46 ± 0.38	66.08 ± 0.84	19.72 ± 0.48
CROMOTEX$_{\text{(no SSL, no AHNP)}}$	74.66 ± 0.10	31.19 ± 0.28	76.23 ± 0.19	19.40 ± 0.08	72.18 ± 0.09	22.01 ± 0.20
CROMOTEX$_{\text{(no AHNP)}}$	74.73 ± 0.11	31.72 ± 0.14	76.78 ± 0.10	18.76 ± 0.12	71.78 ± 0.23	21.28 ± 0.34
CROMOTEX$_{\text{(no SSL)}}$	73.08 ± 0.01	29.67 ± 0.10	77.98 ± 0.30	17.13 ± 0.11	72.09 ± 0.31	22.82 ± 0.42
CroMoTEX (ours)	$\mathbf{75.23 \pm 0.04}$	$\mathbf{31.90 \pm 0.21}$	$\mathbf{78.31 \pm 0.25}$	$\mathbf{22.39 \pm 0.83}$	$\mathbf{75.51 \pm 0.32}$	$\mathbf{29.17 \pm 0.41}$
Direct Classif. (CXR)	86.27 ± 0.18	45.70 ± 0.14	93.62 ± 0.13	47.45 ± 0.21	93.59 ± 0.23	61.25 ± 0.19

Table 2: Comparison of adaptive hard negative penalization strategies (`topk`, `linear`, `exp`) across three pathologies.

Pathology	`topk`	`linear`	`exp`
	AUROC		
Cardiomegaly	$\mathbf{75.23 \pm 0.04}$	73.92 ± 0.12	75.02 ± 0.08
Edema	77.55 ± 0.23	77.89 ± 0.18	$\mathbf{78.31 \pm 0.25}$
Pleural Effusion	$\mathbf{75.51 \pm 0.32}$	74.29 ± 0.11	74.40 ± 0.32
	F1		
Cardiomegaly	$\mathbf{31.90 \pm 0.21}$	30.28 ± 0.16	30.92 ± 0.18
Edema	20.19 ± 0.62	21.34 ± 0.18	$\mathbf{22.39 \pm 0.83}$
Pleural Effusion	$\mathbf{29.17 \pm 0.41}$	25.69 ± 0.48	27.54 ± 0.28

4.1 Datasets

We perform experiments using the MIMIC-IV family of datasets (Johnson et al., 2023; Goldberger et al., 2000) consisting of: MIMIC-IV-ECG, a dataset of approximately $800,000$

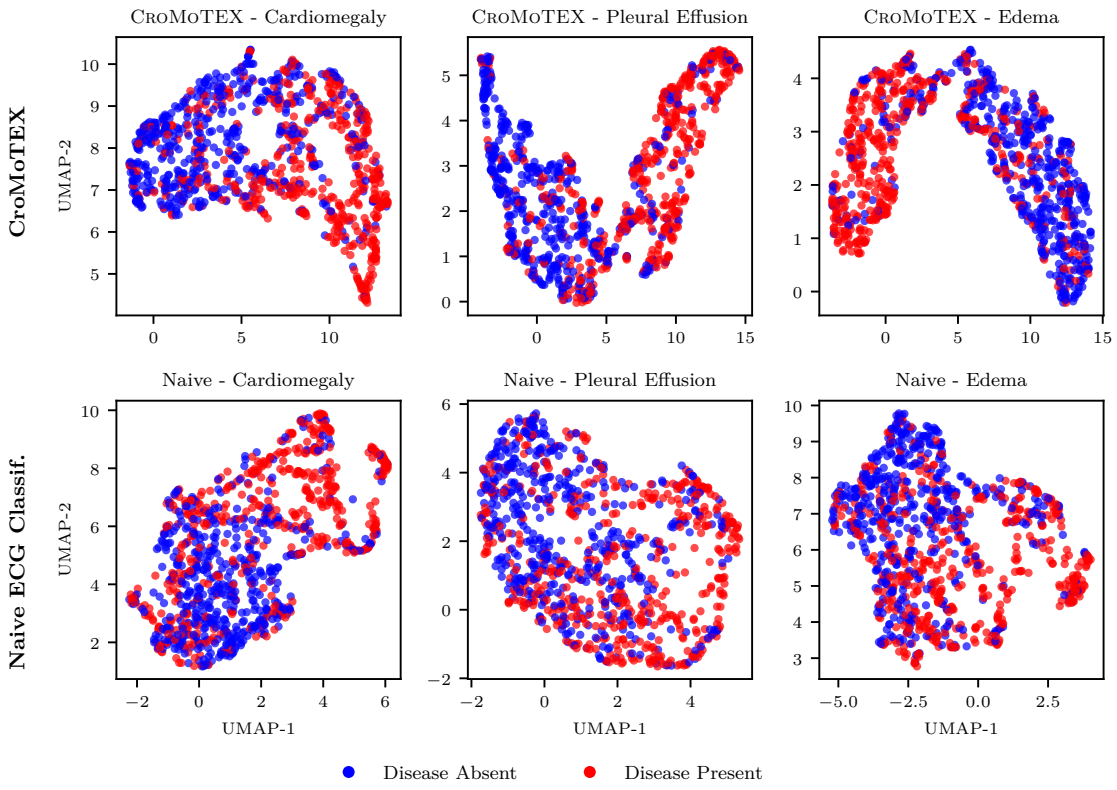


Figure 2: UMAP (McInnes et al., 2018) projections of ECG embeddings from our proposed model (CroMoTEX) versus a naive ECG classification baseline. The embeddings produced by CroMoTEX exhibit improved class separation, reflecting more semantically structured representations. This aligns with the superior classification performance reported in Table 1.

Table 3: Summary of hyper-parameters used for the proposed model.

ECG Encoder (Architecture)		**Cross-modal Alignment**	
Input Shape	[12, 1000]	Batch Size	256
Kernel Size	5	LR (Peak)	10^{-4}
Stride1	5	LR (Start)	10^{-5}
Stride2	1	Sched.	Cos Ann. w/ LR
Intmdt. Dim	128	Temp. τ	0.01
Embed Dim	256	AHNP	`topk, exp`
Num Heads	8	AHNP k	7.5%
Num Layers	4	AHNP α	4.5
Activ. (Conv1D)	ReLU	Pos. Pair Wt. β	3
Activ. (Transf.)	GELU	Wt. Decay	10^{-5}
Classif. Dim.	256	**Fine-tuning**	
Classif. Layers	4	Batch Size	256
Classif. Dropout	0.1	LR (Peak)	10^{-5}
		LR (Start)	10^{-6}
		Sched.	Cos Ann. w/ LR
		Loss	Cross-Entropy
		Optimizer	Adam

diagnostic electrocardiograms; MIMIC-CXR (Johnson et al., 2019), a dataset of 377,110 chest X-rays with associated radiology reports, and disease labels derived from CheXpert labeler, which serves as the imaging dataset in our experiments; and MIMIC-IV which serves as the core patient database helping us link chest X-rays to the corresponding ECGs. We merge the three datasets to obtain a single table $\mathcal{T}_{\text{full}} : \{(e_i, x_i, y_i, \texttt{subject_id}_i)\}_{i=1}^{N}$, where `subject_id` uniquely identifies a patient. Note that $\mathcal{T}_{\text{full}}$ contains rows with missing ECGs e_i, as not every patient who had a chest X-ray also had an ECG during the same hospital visit. We then perform a random train-validation-test split of 70 : 10 : 20 on unique `subject_id`s to obtain the training ($\mathcal{T}_{\text{full}}^{\text{train}}$), validation ($\mathcal{T}_{\text{full}}^{\text{val}}$) and testing ($\mathcal{T}_{\text{full}}^{\text{test}}$) data splits. For performing cross-modal alignment, we obtain paired subsets of the training and validation data by dropping rows with missing ECGs: $\mathcal{T}_{\text{paired}}^{\text{split}} = \{(e, x, y, \texttt{subject_id}) : e \neq \texttt{NULL}, (e, x, y, \texttt{subject_id}) \in \mathcal{T}_{\text{full}}^{\text{split}}\}$ for split $\in \{\text{train}, \text{val}\}$. For self-supervised pre-training of the ECG encoder, we create training and validation datasets $\mathcal{T}_{\text{ecg}}^{\text{train}}$ and $\mathcal{T}_{\text{ecg}}^{\text{val}}$ consisting of all ECGs in MIMIC-IV-ECG, except those belonging to `subject_id`s present in $\mathcal{T}_{\text{full}}^{\text{test}}$.

We pre-process the raw ECGs by first down-sampling to 100 Hz. We then remove baseline-wander (Lenis et al., 2017; Thapa et al., 2024) and normalize each ECG lead to the range $[-1, 1]$ to obtain an array of shape `[12, 1000]`. For the self-supervised pre-training of ECG encoder (Fig. 1), we utilize the augmentations based on vector-cardiogram (VCG) (Gopal et al., 2021). A VCG is obtained from an ECG through the inverse Dower's transform D^{-1} (Gopal et al., 2021), and represents the electrical activity of the heart in 3D spatial coordinates. We obtain an augmented ECG as $\text{V}(e_i) = DSRD^{-1}(e_i)$ where D and D^{-1} represent the Dower's and inverse Dower's transform respectively, $S \in \mathbb{R}^{3\times3}$ is a

random scaling matrix and $R \in \mathbb{R}^{3\times3}$ is a random rotation matrix. We then apply random time masking on the resulting ECG. In the cross-modal alignment stage, we use the time-domain ECG augmentations proposed in (Raghu et al., 2022). We convert the chest X-ray images to gray scale, re-normalize pixel values to the range $[-1024, 1024]$, perform center crop, and resize them to 224×224 pixels.

4.2 Results: Cross-Modal Transfer for ECG-Based Diagnosis

As shown in Fig. 1, we perform pre-training, cross-modal alignment, and fine-tuning to learn ECG representations using chest X-ray-derived knowledge. We evaluate CroMoTEX on the downstream classification task of detecting three different pathologies using ECG alone: Cardiomegaly, Edema and Pleural Effusion. We use the following metrics to evaluate classification performance: AUROC (Area Under Receiver Operating Characteristics curve) and F1 score (harmonic mean of precision and recall).

Baselines and Ablations: Given the limited prior research on cross-modal transfer between chest X-rays and ECGs, we evaluate our approach by comparing CroMoTEX against the following baselines: **SupCon** (Khosla et al., 2020), a contrastive learning framework that adds explicit supervision from labels to enhance task-relevant representation learning; **ECCL** (Ding et al., 2024) and **Cross-modal AE** (Radhakrishnan et al., 2023) which are cross-modal transfer frameworks from Cardiac Magnetic Resonance (CMR) images to ECGs; **BIOT** (Yang et al., 2023), a Transformer-based architecture for bio-signals such as ECGs; and **ResNet-1D**, a popular architecture choice for encoding ECGs (Liu et al., 2024). In addition to these comparisons, we conduct ablation studies to systematically examine the contributions of key components in our framework.

As seen in Table 1, CroMoTEX outperforms the baseline models in the classification of all three pathologies, under both AUROC and F1 score metrics. These results show that our approach significantly improves the detection of these pathologies over direct ECG-based classification, as a result of the cross-modal alignment with CXR. The use of SupCon loss, instead of our AHNP loss with the same architecture yields close, second best results, showing the benefits of supervised alignment in downstream classification performance. On the other hand ECCL and Cross-modal AE, which do not use supervision from the labels, do not deliver good classification performance. Although ECCL combines contrastive loss and classification loss during alignment, this leads to poorer results than using explicit supervision in the contrastive objective. BIOT (Biosignal Transformer) and ResNet-1D are other popular choices for encoding ECGs. As both BIOT and CroMoTEX use a Transformer as part of ECG encoder backbone, BIOT's under-performance indicates the efficacy of our patch embedding convolution layers described in Sec. 3.3. While purely convolution-based architectures such as ResNet-1D have been successfully used for encoding ECGs, we see that the Transformer-based CroMoTEX performs significantly better across the three pathologies, leading us to believe that the attention mechanism helps achieve superior encoding of spatiotemporal relations in an ECG.

In addition to quantitative metrics, we visualize the structure of the learned ECG embeddings using UMAP (McInnes et al., 2018) projections in Fig. 2. For each pathology, we compare embeddings from a naive ECG classifier with those produced by CroMoTEX after cross-modal alignment with chest X-rays and subsequent fine-tuning as described in

Sec. 3.3. The projections reveal that CROMOTEX yields significantly improved class separation in the latent space, with visibly more distinct clustering of positive and negative samples. In contrast, the naive classifier produces relatively poorly structured embeddings. These observations provide qualitative support for the effectiveness of our contrastive alignment strategy, and further corroborate the improvements seen in classification performance.

To further understand the impact of different adaptive hard negative penalization (AHNP) strategies, we compare the performance of `topk`, `linear`, and `exp` weighting schemes across three pathologies in Table 2. We observe that the `topk` strategy yields the best AUROC and F1 scores for Cardiomegaly and Pleural Effusion, indicating its effectiveness in these relatively well-separated tasks. Interestingly, the `exp` strategy outperforms the others for Edema, suggesting that its emphasis on progressively harder negatives may be better suited for subtler or less separable conditions. While the optimal AHNP strategy may vary by pathology, we find that using `topk` consistently across all tasks still achieves performance highly competitive with the best baseline per pathology. These results demonstrate the flexibility of our framework to accommodate multiple modes of hard negative penalization and highlight `topk` as a strong default choice.

Finally, the ablations (Table 1) clearly outline the key contributions of various components of our framework and training strategy. We see that both AHNP and the Self-Supervised Learning (SSL pre-training, described in Sec. 3.3.1) of ECG encoder play a crucial role in improving the performance of CROMOTEX. While neither component alone helps us outperform the baselines, SSL pre-training combined with cross-modal alignment using AHNP loss help us achieve state-of-the-art performance across all three diseases.

5 Discussion

Our findings have meaningful clinical implications, particularly in the context of expanding access to early diagnostics. While chest X-rays remain the gold standard for diagnosing conditions like cardiomegaly, pleural effusion, and edema, their limited availability in non-hospital settings poses a barrier to timely detection. ECGs, on the other hand, are more readily acquired–nowadays via wearable smart devices–making them attractive for large-scale, accessible screening. By transferring diagnostic knowledge from CXRs to ECGs, CROMOTEX enables improved ECG-based detection of these conditions, potentially supporting earlier intervention in resource-constrained or ambulatory care scenarios.

In evaluating CROMOTEX across multiple cardiopulmonary pathologies, we observe consistent improvements over strong baselines such as ECCL, Cross-Modal Autoencoders, and BIOT. The combination of self-supervised ECG pretraining with our novel AHNP-based supervised contrastive loss enables more task-relevant and robust ECG representations. These improvements are not only quantitative but also evident in qualitative embedding separability, as seen in our UMAP visualizations.

6 Conclusion

We introduced CROMOTEX, a supervised cross-modal learning framework that transfers diagnostic knowledge from chest X-rays to ECGs to improve ECG-based disease detection. By incorporating label supervision and our proposed AHNP loss, CROMOTEX achieves

state-of-the-art performance on multiple cardiopulmonary pathologies and outperforms existing baselines. Our ablation studies confirm the complementary roles of self-supervised ECG pretraining and adaptive contrastive alignment in achieving these gains.

However, despite these advances, we observe a significant performance gap between our cross-modal transfer model and direct CXR-based classification, indicating room for further improvements in ECG-CXR alignment. Bridging this gap through enhanced alignment strategies, better modality fusion techniques, or larger-scale multimodal pretraining remains a promising direction for future research.

References

T. Chen, S. Kornblith, M. Norouzi, and G. Hinton. A Simple Framework for Contrastive Learning of Visual Representations. In *Proceedings of the 37th International Conference on Machine Learning*, pages 1597–1607. PMLR, Nov. 2020.

J. Y. Cheng, H. Goh, K. Dogrusoz, O. Tuzel, and E. Azemi. Subject-aware contrastive learning for biosignals. *arXiv preprint arXiv:2007.04871*, 2020.

J. P. Cohen, J. D. Viviano, P. Bertin, P. Morrison, P. Torabian, M. Guarrera, M. P. Lungren, A. Chaudhari, R. Brooks, M. Hashir, et al. Torchxrayvision: A library of chest x-ray datasets and models. In *International Conference on Medical Imaging with Deep Learning*, pages 231–249. PMLR, 2022.

Z. Ding, Y. Hu, Z. Li, H. Zhang, F. Wu, Y. Xiang, T. Li, Z. Liu, X. Chu, and Z. Huang. Cross-Modality Cardiac Insight Transfer: A Contrastive Learning Approach to Enrich ECG with CMR Features. In *Medical Image Computing and Computer Assisted Intervention – MICCAI 2024*, pages 109–119. Springer Nature Switzerland, 2024.

A. L. Goldberger, L. A. Amaral, L. Glass, J. M. Hausdorff, P. C. Ivanov, R. G. Mark, J. E. Mietus, G. B. Moody, C.-K. Peng, and H. E. Stanley. Physiobank, physiotoolkit, and physionet: components of a new research resource for complex physiologic signals. *Circulation*, 101(23):e215–e220, 2000.

B. Gopal, R. Han, G. Raghupathi, A. Ng, G. Tison, and P. Rajpurkar. 3KG: Contrastive Learning of 12-Lead Electrocardiograms using Physiologically-Inspired Augmentations. In *Proceedings of Machine Learning for Health*, pages 156–167. PMLR, Nov. 2021.

J.-B. Grill, F. Strub, F. Altché, C. Tallec, P. Richemond, E. Buchatskaya, C. Doersch, B. Avila Pires, Z. Guo, M. Gheshlaghi Azar, et al. Bootstrap your own latent-a new approach to self-supervised learning. *Advances in neural information processing systems*, 33:21271–21284, 2020.

P. Hager, M. J. Menten, and D. Rueckert. Best of Both Worlds: Multimodal Contrastive Learning With Tabular and Imaging Data. *Proceedings of the IEEE/CVF Conference on Computer Vision and Pattern Recognition*, pages 23924–23935, 2023.

N. Hayat, K. J. Geras, and F. E. Shamout. MedFuse: Multi-modal fusion with clinical time-series data and chest X-ray images, Mar. 2023.

K. He, H. Fan, Y. Wu, S. Xie, and R. Girshick. Momentum contrast for unsupervised visual representation learning. In *Proceedings of the IEEE/CVF conference on computer vision and pattern recognition*, pages 9729–9738, 2020.

S.-C. Huang, L. Shen, M. P. Lungren, and S. Yeung. GLoRIA: A Multimodal Global-Local Representation Learning Framework for Label-Efficient Medical Image Recognition. *Proceedings of the IEEE/CVF International Conference on Computer Vision*, pages 3942–3951, 2021.

C. Jia, Y. Yang, Y. Xia, Y.-T. Chen, Z. Parekh, H. Pham, Q. Le, Y.-H. Sung, Z. Li, and T. Duerig. Scaling up visual and vision-language representation learning with noisy text supervision. In *International conference on machine learning*, pages 4904–4916. PMLR, 2021.

A. E. Johnson, T. J. Pollard, S. J. Berkowitz, N. R. Greenbaum, M. P. Lungren, C.-y. Deng, R. G. Mark, and S. Horng. Mimic-cxr, a de-identified publicly available database of chest radiographs with free-text reports. *Scientific data*, 6(1):317, 2019.

A. E. Johnson, L. Bulgarelli, L. Shen, A. Gayles, A. Shammout, S. Horng, T. J. Pollard, S. Hao, B. Moody, B. Gow, et al. Mimic-iv, a freely accessible electronic health record dataset. *Scientific data*, 10(1):1, 2023.

P. Khosla, P. Teterwak, C. Wang, A. Sarna, Y. Tian, P. Isola, A. Maschinot, C. Liu, and D. Krishnan. Supervised Contrastive Learning. In *Advances in Neural Information Processing Systems*, volume 33, pages 18661–18673. Curran Associates, Inc., 2020.

R. King, T. Yang, and B. J. Mortazavi. Multimodal Pretraining of Medical Time Series and Notes. In *Proceedings of the 3rd Machine Learning for Health Symposium*, pages 244–255. PMLR, Dec. 2023.

D. Kiyasseh, T. Zhu, and D. A. Clifton. Clocs: Contrastive learning of cardiac signals across space, time, and patients. In *International Conference on Machine Learning*, pages 5606–5615. PMLR, 2021.

G. Lenis, N. Pilia, A. Loewe, W. H. Schulze, and O. Dössel. Comparison of baseline wander removal techniques considering the preservation of st changes in the ischemic ecg: a simulation study. *Computational and mathematical methods in medicine*, 2017(1): 9295029, 2017.

C. Liu, Z. Wan, C. Ouyang, A. Shah, W. Bai, and R. Arcucci. Zero-Shot ECG Classification with Multimodal Learning and Test-time Clinical Knowledge Enhancement. In *Forty-First International Conference on Machine Learning*, June 2024.

J. Liu, G. Zhao, Y. Fei, M. Zhang, Y. Wang, and Y. Yu. Align, attend and locate: Chest x-ray diagnosis via contrast induced attention network with limited supervision. In *Proceedings of the IEEE/CVF International Conference on Computer Vision*, pages 10632–10641, 2019.

L. McInnes, J. Healy, and J. Melville. Umap: Uniform manifold approximation and projection for dimension reduction. *arXiv preprint arXiv:1802.03426*, 2018.

A. v. d. Oord, Y. Li, and O. Vinyals. Representation learning with contrastive predictive coding. *arXiv preprint arXiv:1807.03748*, 2018.

A. Radford, J. W. Kim, C. Hallacy, A. Ramesh, G. Goh, S. Agarwal, G. Sastry, A. Askell, P. Mishkin, J. Clark, G. Krueger, and I. Sutskever. Learning Transferable Visual Models From Natural Language Supervision. In *Proceedings of the 38th International Conference on Machine Learning*, pages 8748–8763. PMLR, July 2021.

A. Radhakrishnan, S. F. Friedman, S. Khurshid, K. Ng, P. Batra, S. A. Lubitz, A. A. Philippakis, and C. Uhler. Cross-modal autoencoder framework learns holistic representations of cardiovascular state. *Nature Communications*, 14(1):2436, Apr. 2023. ISSN 2041-1723. doi: 10.1038/s41467-023-38125-0. URL https://www.nature.com/articles/s41467-023-38125-0.

A. Raghu, D. Shanmugam, E. Pomerantsev, J. Guttag, and C. M. Stultz. Data augmentation for electrocardiograms. In *conference on health, inference, and learning*, pages 282–310. PMLR, 2022.

H. Sowrirajan, J. Yang, A. Y. Ng, and P. Rajpurkar. MoCo Pretraining Improves Representation and Transferability of Chest X-ray Models. In *Proceedings of the Fourth Conference on Medical Imaging with Deep Learning*, pages 728–744. PMLR, Aug. 2021.

S. Thapa, K. Howlader, S. Bhattacharjee, and W. le. MoRE: Multi-Modal Contrastive Pre-training with Transformers on X-Rays, ECGs, and Diagnostic Report, Oct. 2024.

A. Vaswani, N. Shazeer, N. Parmar, J. Uszkoreit, L. Jones, A. N. Gomez, Ł. Kaiser, and I. Polosukhin. Attention is all you need. *Advances in neural information processing systems*, 30, 2017.

C. Yang, M. B. Westover, and J. Sun. BIOT: Biosignal Transformer for Cross-data Learning in the Wild. *37th Conference on Neural Information Processing Systems (NeurIPS 2023)*, 2023.

W. Yao, K. Yin, W. K. Cheung, J. Liu, and J. Qin. DrFuse: Learning Disentangled Representation for Clinical Multi-Modal Fusion with Missing Modality and Modal Inconsistency. *Proceedings of the AAAI Conference on Artificial Intelligence*, 38(15):16416–16424, Mar. 2024. ISSN 2374-3468.